

Supplementary Information for

Developing effective strategy to suppress dark current for high-performance planar photodetectors

Bin Tang,^{a,b,c} Mingxin Sun,^{a,b,c} Tong Liu,^{b,c,d} Junjie Wang,^{*a,b,c} Jianxiao Wang,^{b,c,d} Xiaofei Qu,^{*a} and Xichang Bao^{*a,b,c,d}

^a College of Materials Science and Engineering, Qingdao University of Science and Technology, Qingdao 266071, China quxiaofei@qust.edu.cn

^b Key Laboratory of Photoelectric Conversion and Utilization of Solar Energy, Qingdao Institute of Bioenergy and Bioprocess Technology, Chinese Academy of Sciences, Qingdao 266101, China baoxc@qibebt.ac.cn; wangjj2021@qibebt.ac.cn

^c Laboratory of Solar Energy, Shandong Energy Institute, Qingdao 266101, China

^d Qingdao New Energy Shandong Laboratory, Qingdao 266101, China

Detailed device preparation

Prior to preparing the OPD devices, the ITO glass was ultrasonicated for 15 minutes using ITO-specific detergent, deionized water, acetone, deionized water, and isopropyl alcohol in order to remove impurities from the substrate. The isopropanol adhering to the ITO was blown dry with ultra-dry nitrogen, followed by plasma oxygen treatment for 200 s. Then PEDOT:PSS was spin-coated at 4000 rpm for 30 s to form an approximately 30 nm thick film, and finally annealed in air at 155 °C for 15 min before being transferred into a glove box for the next step of the process.

For BC devices, PM6 and BO-4Cl were prepared in a 1:1.2 ratio, with a solution concentration of 7.4 mg/ml for thin-film devices and 8.4 mg/ml for thick-film devices, and spun coated onto the previously treated substrates at 3000 rpm.

For the thin-film SD devices, the concentration of PM6 was 7.4 mg/ml and BO-4Cl was 8 mg/ml; the concentration of PM6 in the thick-film SD devices was 10 mg/ml and BO-4Cl was 10 mg/ml. For SD OPD devices with P(VDF-TrFE) was introduced, P(VDF-TrFE) was dissolved in THF at solution concentrations of 0.5, 1, and 1.5 mg/ml and spin-coated on the donor layer at 3000 rpm.

After the preparation of the active layer as described above, it was placed on a heating table for annealing at 100 °C for 9 min (We explored a range of annealing treatments and concluded that 100 °C for 9 min is the optimal annealing condition, as shown in Fig. S1). Finally, PDINN was spin-coated on the active layer as an electron transport layer and 90 nm thick Ag electrodes were vaporized.

Space charge limiting current (SCLC) method

The electron mobility of different devices was measured using electron-only devices (ITO/ZnO/Active layer/PDINN/Ag). The prepared ZnO precursor solution was dissolved in a glove box overnight, then spin-coated on ITO at 3000 rpm, annealed at 150 °C in air for 30 min and transferred back to the glove box for spin-coating of the active layer and the electron transport layer PDINN, and finally the Ag electrode was vapor-deposited.

The hole mobility of different devices was measured using hole-only devices (ITO/PEDOT:PSS/Active layer/MoO₃/Ag). After spin-coating PEDOT:PSS on ITO at 4000 rpm, it was annealed at 155 °C 15 min in air and then transferred to glove box for spin-coating of the active layer, and finally vaporized the hole-transport layer (MoO₃) and Ag electrode.

The mobility was extracted by fitting the current density-voltage curves using space charge limited current (SCLC), which is described by the equation

$$J = \frac{9}{8} \epsilon_0 \epsilon_r \mu_h \frac{V^2}{d^3}$$

where J is the current density, ϵ_0 represents the vacuum dielectric constant, and ϵ_r represents the dielectric constant of organic materials (generally taken to be around 4), μ_h is the zero-filed mobility, V is the effective voltage and d is the thickness of the organic layer. The effective voltage can be obtained by subtracting the built-in voltage (V_{bi}) and the voltage drop (V_s) from the substrate's series resistance from the applied voltage (V_{appl}): $V = V_{appl} - V_{bi} - V_s$. The hole and electron mobilities can be calculated from the slope of the $J^{1/2}$ - V curves.

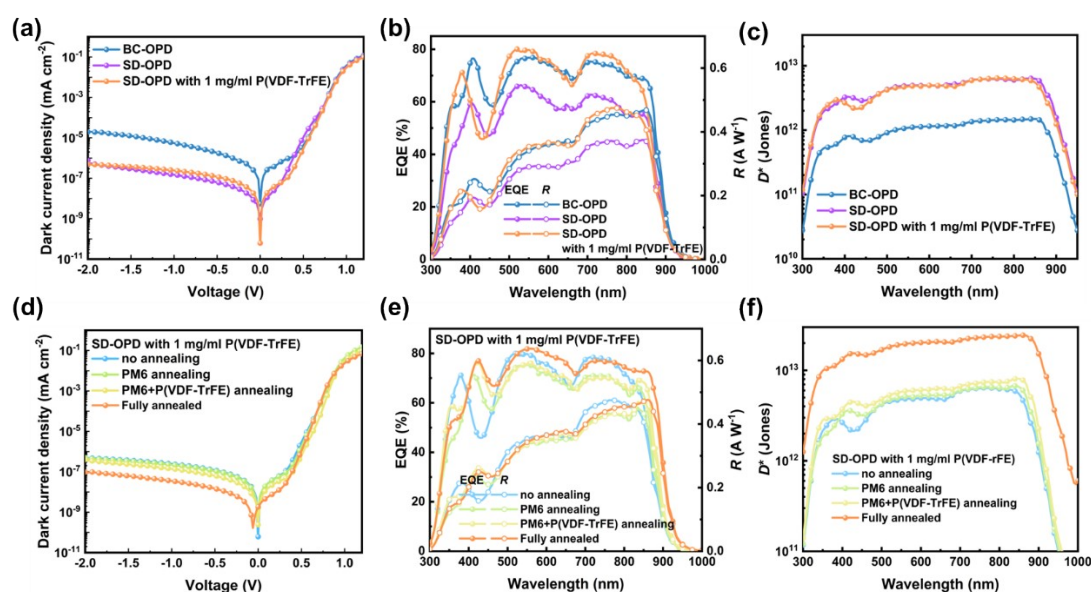


Fig. S1 The dark current density (a), EQE and R (b), D^* (c) for three unannealed devices; Dark current density (d), EQE and R (e), D^* (f) of SD-OPD with 1 mg/ml P(VDF-TrFE) devices under different annealing conditions.

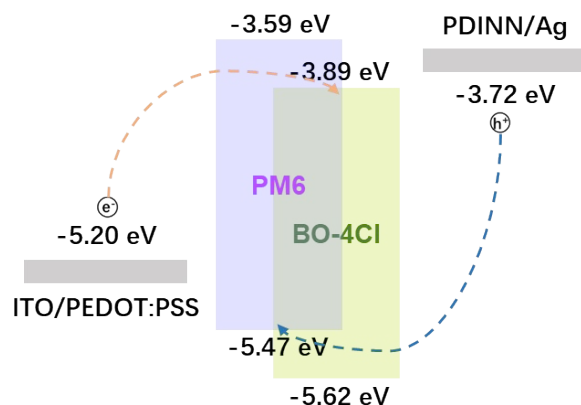


Fig. S2 Schematic of the energy level and reverse carrier injection of BC OPD device.

Table S1 Dark current density of different devices under different bias voltages. (The unit of dark current density is A cm^{-2})

Devices		Applied voltage				
		-0.1 V	-0.5 V	-1 V	-1.5 V	-2 V
Thin	BC	1.08×10^{-5}	7.29×10^{-5}	2.37×10^{-4}	4.47×10^{-4}	7.15×10^{-4}
	SD	1.02×10^{-6}	7.01×10^{-6}	2.15×10^{-5}	5.21×10^{-5}	6.17×10^{-5}
Thick	BC	2.83×10^{-8}	3.28×10^{-7}	1.51×10^{-6}	3.87×10^{-6}	7.84×10^{-6}
	SD	8.60×10^{-9}	7.71×10^{-8}	2.77×10^{-7}	7.16×10^{-7}	1.21×10^{-6}

Table S2 Summary table of the characteristics of the variation of the optical current density with the effective voltage.

Device	J_{SC} (mA cm^{-2})	J_{sat} (mA cm^{-2})	P_{diss} ($J_{\text{SC}}/J_{\text{sat}}$) %
BC-OPD	27.00	28.59	94.4
SD-OPD	26.73	27.52	97.1
SD-OPD with 1mg/ml P(VDF-TrFE)	27.40	27.85	98.4

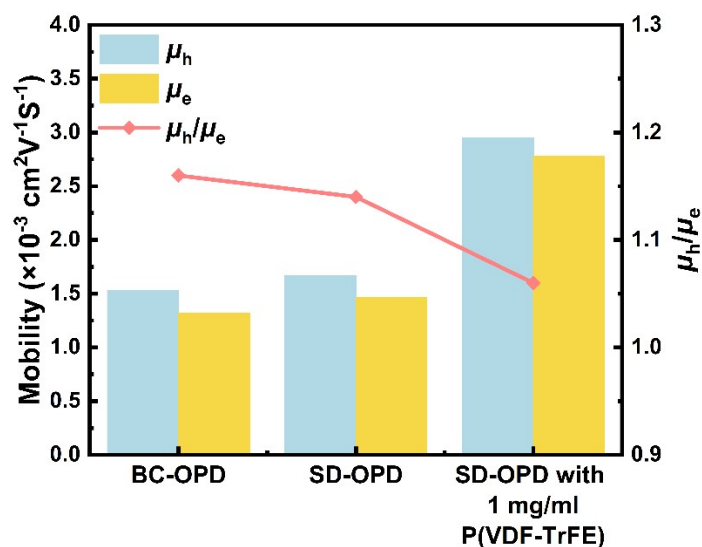


Fig. S3 μ_h , μ_e and μ_h/μ_e of different OPD devices.

Table S3 Electron and hole mobility of OPD devices.

Device	$\mu_h (\times 10^{-3} \text{ cm}^2 \text{ V}^{-1} \text{ s}^{-1})$	$\mu_e (\times 10^{-3} \text{ cm}^2 \text{ V}^{-1} \text{ s}^{-1})$	μ_h/μ_e
BC-OPD	1.53	1.32	1.16
SD-OPD	1.67	1.46	1.14
SD-OPD with 1mg/ml P(VDF-TrFE)	2.95	2.78	1.06

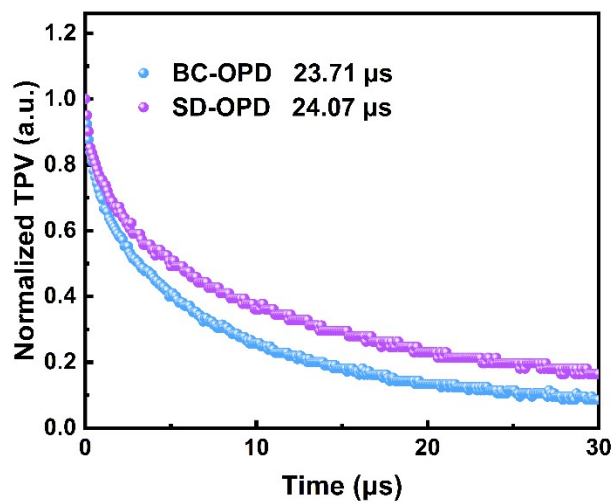


Fig. S4 TPV of different OPD devices.

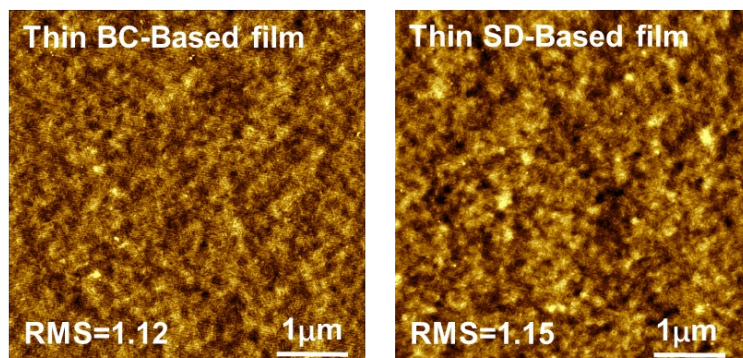


Fig. S5 AFM images of the thin film.

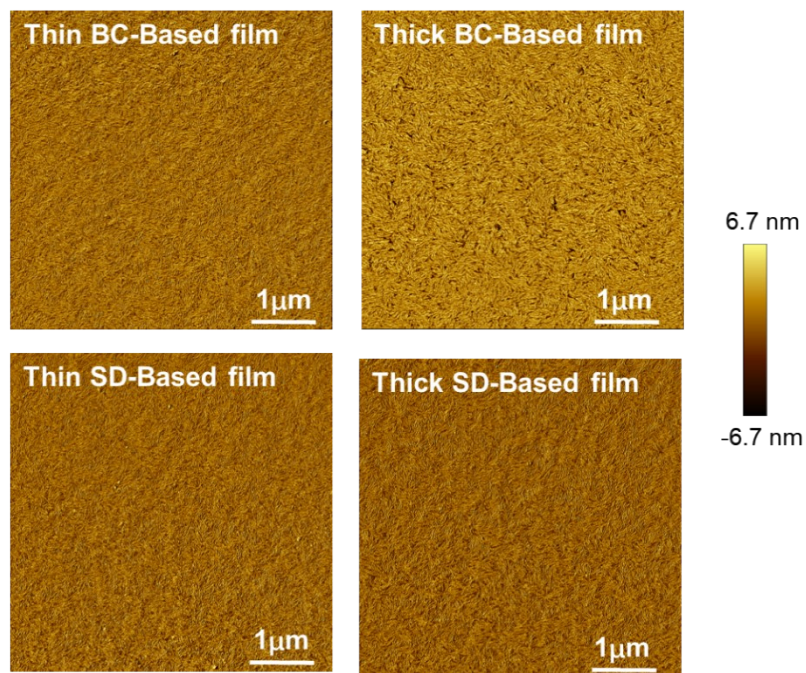


Fig. S6 Phase diagrams of BC-Based and SD-Based films of different thicknesses.

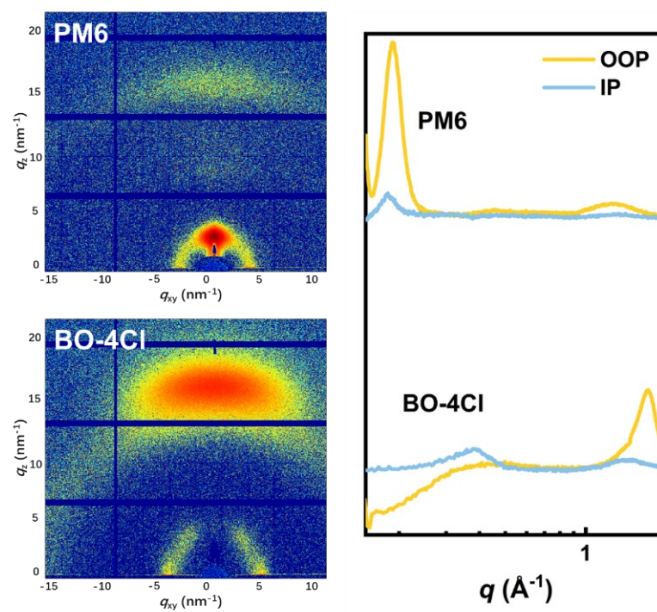


Fig. S7 2D GIWAXS plot of PM6 and BO-4Cl pure film and corresponding 1D line plot.

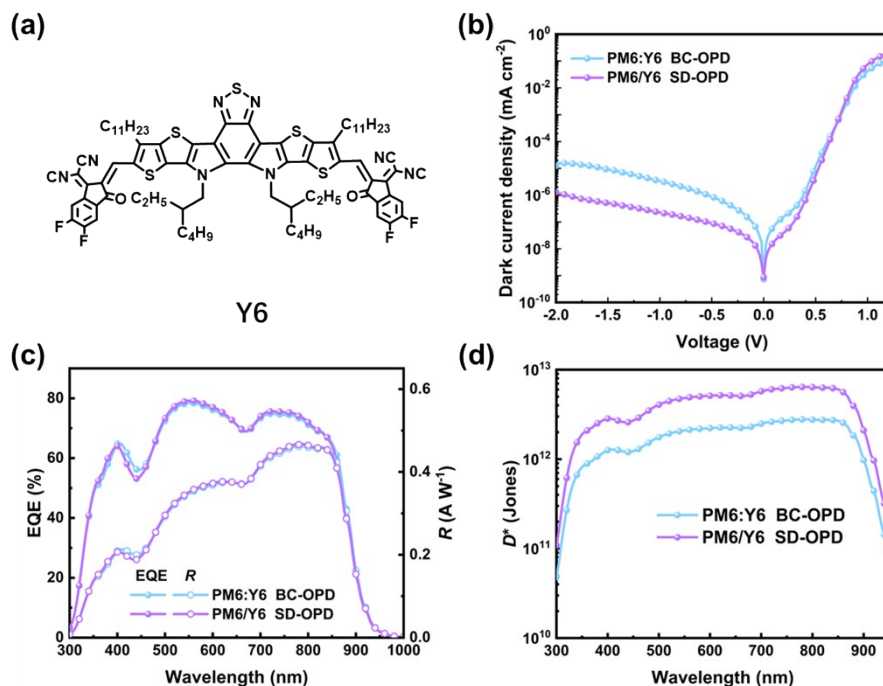


Fig. S8 (a) Chemical structural formula of Y6; (b) J_d of the OPDs; (c) EQE and R of the OPDs; (d) D^* of the OPDs.

Table S4 GIWAXS results and fitting parameters of (010) peaks in OOP direction for pristine and blend films.

Film	Q (\AA^{-1})	d -spacing (\AA)	FWHM (\AA^{-1})	CCL (\AA)
PM6	1.66	3.78	0.321	17.61
BO-4Cl	1.70	3.69	0.235	24.05
P(VDF-TrFE)	1.36	4.62	0.056	100.93
BC-Based film	1.69	3.72	0.256	22.08
SD-Based film	1.72	3.65	0.245	23.07
SD-Based film with 1 mg/ml P(VDF-TrFE)	1.71	3.67	0.217	25.81

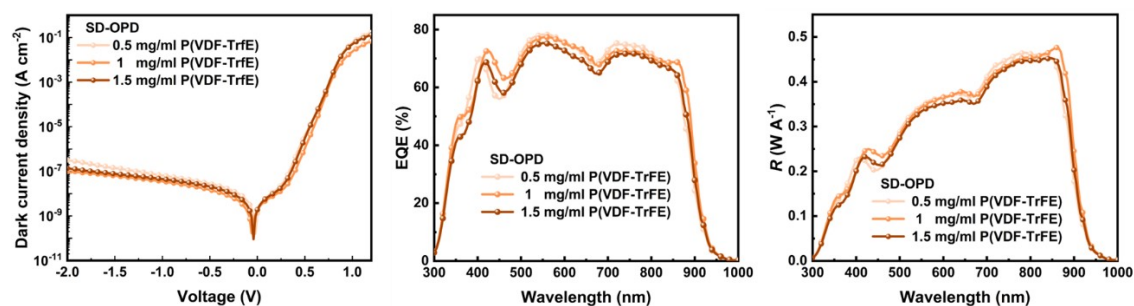


Fig. S9 J_d , EQE and R of SD-OPD with different concentrations of P(VDF-TrFE).

Table S5 Dark current density of SD-OPD with different concentrations of P(VDF-TrFE). (The unit of dark current density is A cm⁻²)

Devices with P(VDF-TrFE) (mg/ml)	Bias voltage				
	-0.1 V	-0.5 V	-1 V	-1.5 V	-2 V
0	8.60×10^{-9}	7.71×10^{-8}	2.77×10^{-7}	7.16×10^{-7}	1.21×10^{-6}
0.5	4.32×10^{-9}	2.76×10^{-8}	6.49×10^{-8}	1.37×10^{-7}	3.21×10^{-7}
1	1.40×10^{-9}	1.48×10^{-8}	3.53×10^{-8}	6.23×10^{-8}	9.73×10^{-8}
1.5	2.62×10^{-9}	2.07×10^{-8}	4.53×10^{-8}	7.78×10^{-8}	1.38×10^{-7}

Table S6 Some performance parameters and recent progress of positive OPD.

Active layer process	Active material	J_d /bias (A cm ⁻²)	R_{\max} (A W ⁻¹)	D^*_{\max} (Jones)	Ref
BC	PM6:Y6	$1.69 \times 10^{-7}/-0.1$ V	0.43	1.86×10^{12}	1
BC	PDPP3T:PC ₇₁ BM	$9.95 \times 10^{-7}/-0.5$ V	0.21	1.03×10^{12}	2
BC	P1:BTP-4Cl	$1.12 \times 10^{-5}/-1$ V	0.02	8.17×10^9	3
SD	PTzBI-Ph/N2200	$1.2 \times 10^{-9}/-0.1$ V	0.25	5.68×10^{12}	4
BC	P1:PCBM	$2.5 \times 10^{-10}/-0.1$ V	0.16	1.40×10^{13}	5
BC	D18:BTP-4F	/	0.27	6.45×10^{12}	6
BC	P3HT:PC ₇₁ BM	$8.09 \times 10^{-10}/0$ V	0.12	6.40×10^{11}	7
BC	PBDB-T:DO-4F	$8.6 \times 10^{-9}/0$ V	0.5	1.51×10^{13}	8
BC	PNTOD:IT-4F	$8.6 \times 10^{-9}/-0.1$ V	0.32	1.32×10^{13}	9
BC	PM6:PDDTYM	$3.88 \times 10^{-9}/0$ V	0.48	1.31×10^{13}	10
BC	NT40:N2200	$2.4 \times 10^{-8}/-0.1$ V	0.26	2.92×10^{12}	11
BC	PTB7-Th:PC ₇₁ BM	$3.55 \times 10^{-9}/0$ V	0.35	1.0×10^{13}	12
SD with P(VDF-TrFE)	PM6/PVDF/BO-4Cl	$1.40 \times 10^{-9}/-0.1$ V	0.47	2.25×10^{13}	This work

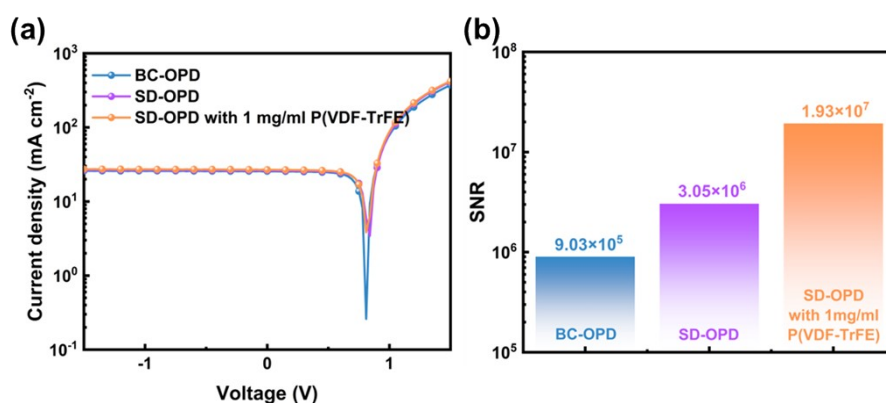


Fig. S10 (a) Photocurrents of OPD devices; (b) SNRs of OPD devices.

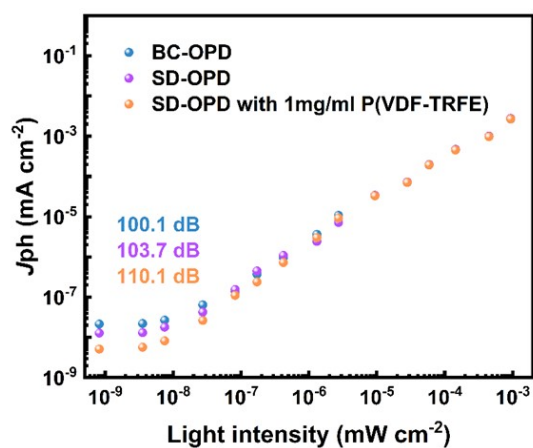


Fig. S11 LDRs of OPD devices.

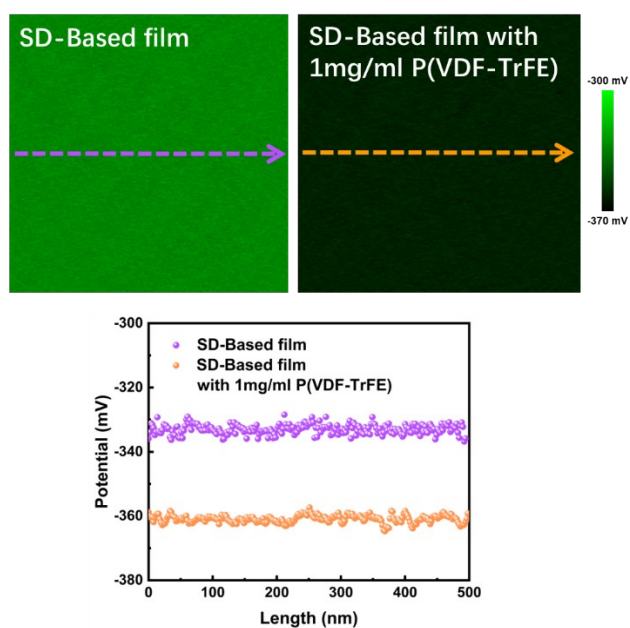


Fig S12 Schematic diagram of the relative potentials along the direction of the arrows.

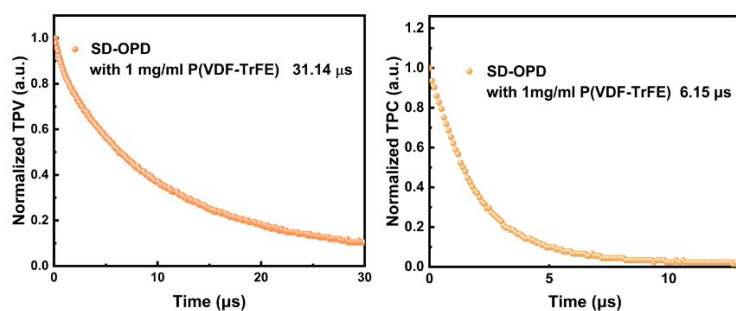


Fig. S13 Normalized TPV and TPC of the SD-based OPD with 1 mg/ml P(VDF-TrFE) devices.

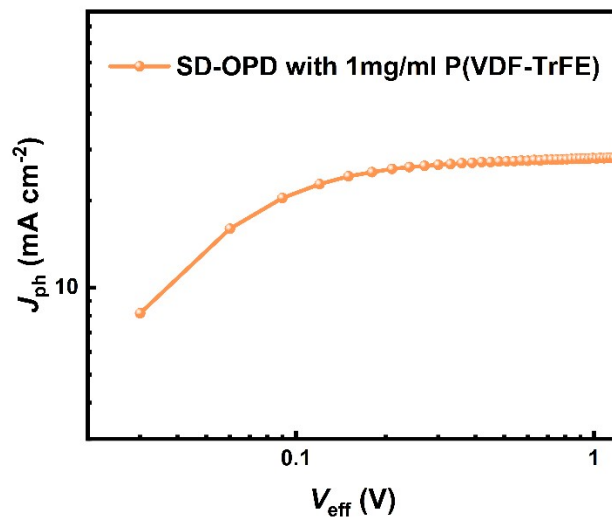


Fig. S14 The Characteristics of the photocurrent density versus effective voltage of SD-OPD with 1 mg/ml P(VDF-TrFE).

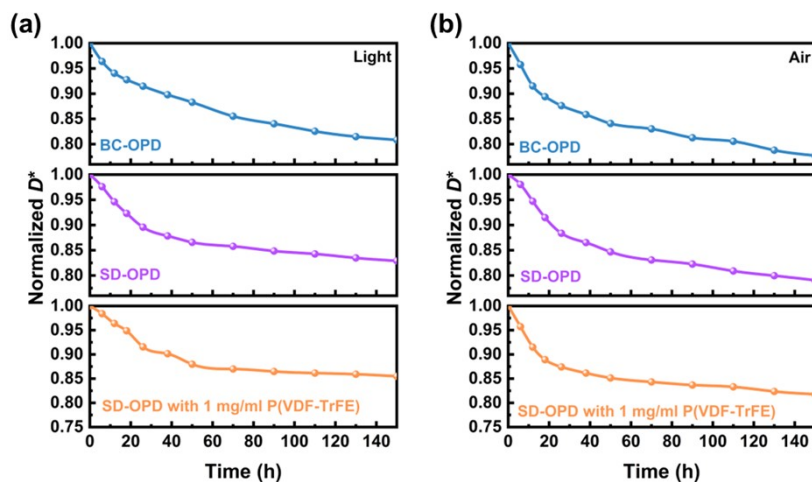


Fig. S15 (a) Light stability of the OPD devices; (b) OPD devices stability in air.

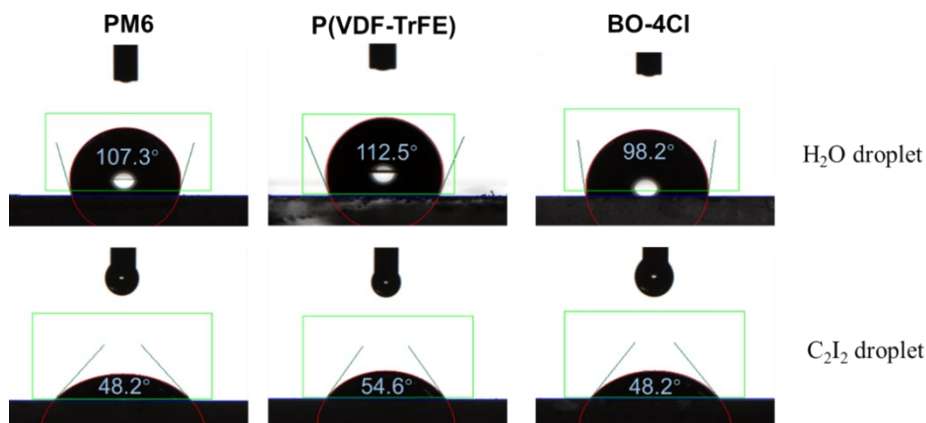


Fig. S16 Contact angle of the PM6, P(VDF-TrFE) and BO-4Cl.

Table S7 Investigations of the contact angles, surface energy of PM6, BO-4Cl and P(VDF-TrFE).

Material	Contact angle		Surface energy (mN m ⁻¹)	χ with PM6	χ with BO-4Cl
	H ₂ O (°)	C ₂ I ₂ (°)			
PM6	107.3	48.2	42.3	-	0.21
P(VDF-TrFE)	112.5	54.6	39.5	0.05	0.06
BO-4Cl	98.2	48.2	36.6	0.21	-

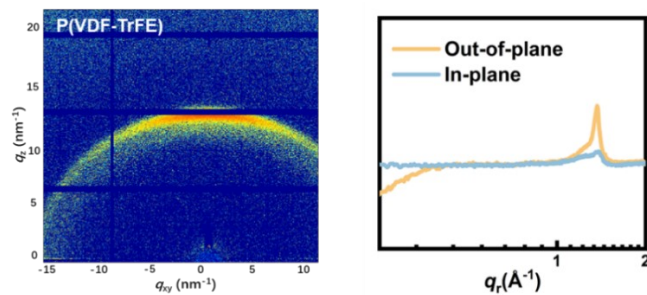


Fig. S17 2D GIWAXS plot of P(VDF-TrFE) pure film and corresponding 1D line plot.

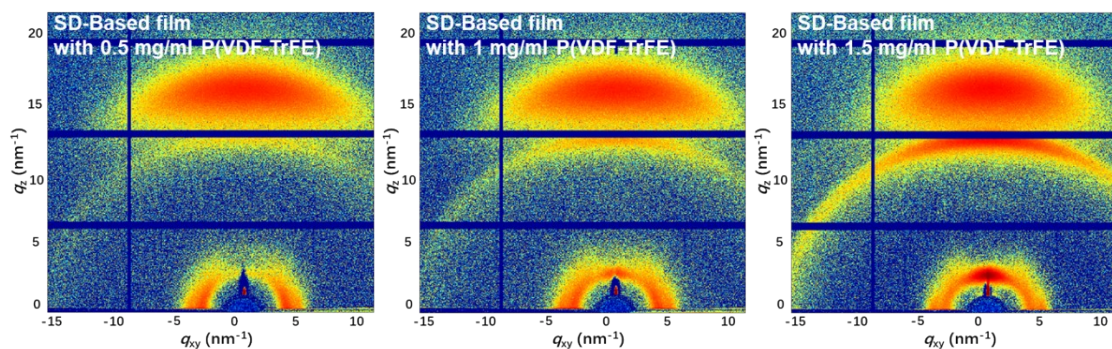


Fig. S18 2D GIWAXS of the SD-Based film with different concentrations of P(VDF-TrFE).

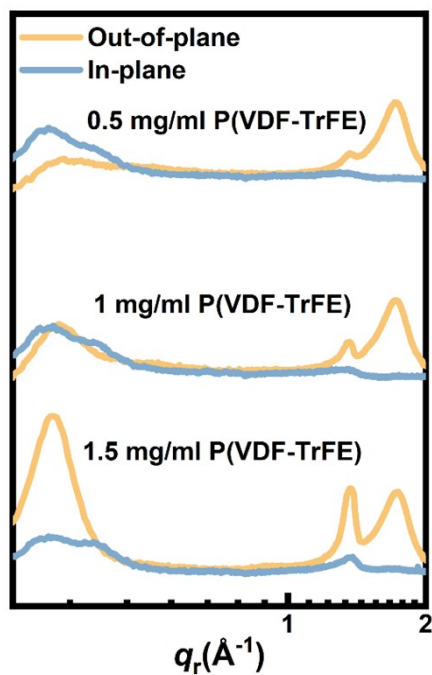


Fig. S19 One-dimensional line graphs corresponding to SD-Based film participating in different concentrations of P(VDF-TrFE).

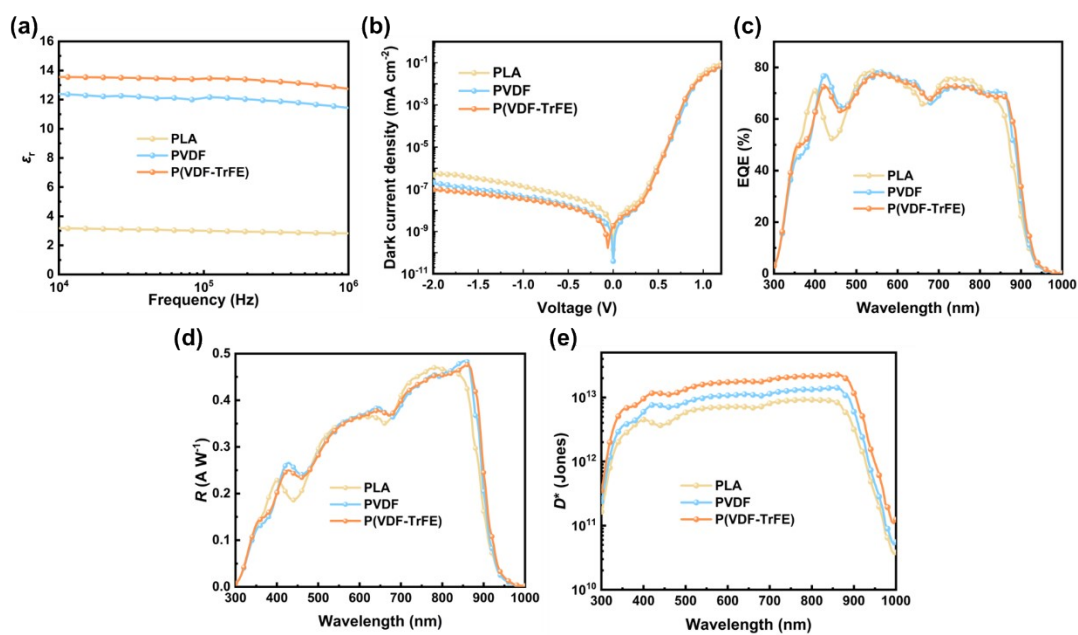
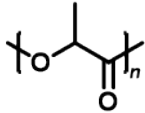
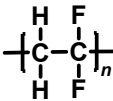
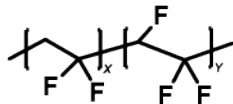


Fig. S20 (a) Dielectric constants of different materials; (b) J_d of the OPDs; (c) EQE of the OPDs; (d) R of the OPDs; (e) D^* of the OPDs.

Table S8 Molecular structural formulae of materials and their dielectric constants.

Material	Molecular formula	Dielectric constant
----------	-------------------	---------------------

PLA		3.2
PVDF		12.3
P(VDF-TrFE)		13.6

1. C. Xu, K. Miao, F. Eisner, G. Liu, C. Feng, H. Su, L. Lan, Z. He and J. Nelson, *Adv. Opt. Mater.*, 2024, **12**, 2302555.
2. X. Zhou, D. Yang and D. Ma, *Adv. Opt. Mater.*, 2015, **3**, 1570-1576.
3. I. Park, C. Kim, R. Kim, N. Li, J. Lee, O. K. Kwon, B. Choi, T. N. Ng and D. S. Leem, *Adv. Opt. Mater.*, 2022, **10**, 2200747.
4. Z. Zhong, L. Bu, P. Zhu, T. Xiao, B. Fan, L. Ying, G. Lu, G. Yu, F. Huang and Y. Cao, *ACS Appl. Mater. Interfaces*, 2019, **11**, 8350-8356.
5. J. Qi, J. Han, X. Zhou, D. Yang, J. Zhang, W. Qiao, D. Ma and Z. Y. Wang, *Macromolecules*, 2015, **48**, 3941-3948.
6. K. Pu, Z. Xu, Y. Gao, C. Zhao, F. Ershad, Y. Li, R. Wang, C. Yu and G. Wei, *Adv. Mater. Technol.*, 2023, **8**, 2300207.
7. J. W. Qiao, F. Z. Cui, L. Feng, P. Lu, H. Yin and X. T. Hao, *Adv. Funct. Mater.*, 2023, **33**, 2301433.
8. Y. Xu, T. Zhang, H. Yao, J. Wang, P. Bi and J. Hou, *J. Energy Chem.*, 2022, **72**, 388-394.
9. Z. Zhong, Z. Zeng, Z. Huang, F. Peng, P. He, L. Lan and L. Ying, *Org. Electron.*, 2022, **109**, 106621.
10. Y. Zheng, Y. Chen, Y. Cao, F. Huang, Y. Guo and X. Zhu, *ACS Mater. Lett.*, 2022, **4**, 882-890.
11. Z. Zhong, K. Li, J. Zhang, L. Ying, R. Xie, G. Yu, F. Huang and Y. Cao, *ACS Appl. Mater. Interfaces*, 2019, **11**, 14208-14214.
12. T. Liu, Z. Jia, Y. Song, N. Yu, Q. Lin, C. Li, Y. Jia, H. Chen, S. Wang, Y. Wei, Y. Lin, F. Huang, Z. Tang, Y. Li, L. Meng and H. Huang, *Adv. Funct. Mater.*, 2023, **33**, 2301167.